Discovery of a selective inhibitor of oncogenic B-Raf kinase with potent antimelanoma activity

James Tsai*, John T. Lee†, Weiru Wang*, Jiazhong Zhang*, Hanna Cho*, Shumeye Mamo*, Ryan Bremer*, Sam Gillette*, Jun Kong†, Nikolas K. Haass†, Katrin Sproesser†, Ling Li†, Keiran S. M. Smalley†, Daniel Fong*, Yong-Liang Zhu*, Adhirai Marimuthu*, Hoa Nguyen*, Billy Lam*, Jennifer Liu*, Ivana Cheung*, Julie Rice*, Yoshihisa Suzuki*, Catherine Luu*, Calvin Settachatgul*, Rafe Shellooe*, John Cantwell*, Sung-Hou Kim‡, Joseph Schlessinger§¶, Kam Y. J. Zhang*, Brian L. West*, Ben Powell*, Gaston Habets*, Chao Zhang*, Prabha N. Ibrahim*, Peter Hirth*, Dean R. Artis*, Meenhard Herlyn†¶, and Gideon Bollag*¶

*Plexxikon, Inc., 91 Bolivar Drive, Berkeley, CA 94710; †Department of Molecular and Cellular Oncogenesis, The Wistar Institute, 3601 Spruce Street, Philadelphia, PA 19104; ‡220 Calvin Laboratory, University of California, Berkeley, CA 94720; and §Department of Pharmacology, Yale University School of Medicine, 333 Cedar Street, New Haven, CT 06520

Contributed by Joseph Schlessinger, December 15, 2007 (sent for review October 15, 2007)

***BRAF*^{V600E} is the most frequent oncogenic protein kinase mutation known. Furthermore, inhibitors targeting "active" protein kinases have demonstrated significant utility in the therapeutic repertoire against cancer. Therefore, we pursued the development of specific kinase inhibitors targeting B-Raf, and the V600E allele in particular. By using a structure-guided discovery approach, a potent and selective inhibitor of active B-Raf has been discovered. PLX4720, a 7-azaindole derivative that inhibits B-Raf^{V600E} with an IC_{50} of 13 nM, defines a class of kinase inhibitor with marked selectivity in both biochemical and cellular assays. PLX4720 preferentially inhibits the active B-Raf^{V600E} kinase compared with a broad spectrum of other kinases, and potent cytotoxic effects are also exclusive to cells bearing the V600E allele. Consistent with the high degree of selectivity, ERK phosphorylation is potently inhibited by PLX4720 in B-Raf^{V600E}-bearing tumor cell lines but not in cells lacking oncogenic B-Raf. In melanoma models, PLX4720 induces cell cycle arrest and apoptosis exclusively in B-Raf^{V600E}-positive cells. In B-Raf^{V600E}-dependent tumor xenograft models, orally dosed PLX4720 causes significant tumor growth delays, including tumor regressions, without evidence of toxicity. The work described here represents the entire discovery process, from initial identification through structural and biological studies in animal models to a promising therapeutic for testing in cancer patients bearing B-Raf^{V600E}-driven tumors.**

cancer | cell signaling | melanoma | phosphorylation | protein kinases

Oncogenic mutations in the *BRAF* gene (1) correlate with increased severity and decreased response to chemotherapy in a wide variety of human tumors (2–4). Hence, direct therapeutic inhibition of oncogenic B-Raf kinase activity affords an avenue to treat these tumors. The therapeutic approach of targeting oncogenic kinase activity has proved very valuable in oncology (5, 6). Recently, we have described the technique termed scaffold-based drug discovery, a strategy for identifying small molecule inhibitors of cyclic nucleotide phosphodiesterases (7). Here, we describe an expansion of this strategy to discover a scaffold targeting protein kinases, and we report the elaboration of this scaffold into the potent and selective B-Raf^{V600E} inhibitor PLX4720.

Because a majority of all melanomas harbor an activating missense mutation (V600E) in the B-Raf oncogene (1), targeted inhibition of the V600E gene product is a particularly rational therapeutic goal in this otherwise therapy-resistant tumor type. Previous generations of B-Raf inhibitors possess Raf inhibitory activity at low nanomolar concentrations (8–13); however, the relative therapeutic efficacy of such inhibitors has been hampered by the lack of bioavailability or by the number of nonspecific targets that are also affected (14, 15). The development of highly specific and effectual inhibitors of the *BRAF*^{V600E} gene product would provide insight into the true therapeutic relevance of this target in malignant melanoma. Here, we demonstrate the preclinical validation of such a compound, PLX4720; this B-Raf^{V600E}-selective inhibitor displays striking antimelanoma activity in both cell- and animal-based model systems.

Results and Discussion

Scaffold- and Structure-Based Discovery of the Inhibitors. To identify protein kinase scaffolds, a selected library of 20,000 compounds ranging in molecular mass between 150 and 350 daltons was screened at a concentration of 200 μM through multiple divergent but structurally characterized kinases, and the screening data were further analyzed to select compounds for cocrystallography. For instance, out of the library, 238 compounds inhibited the activity of the three kinases, Pim-1, p38, and CSK, by at least 30% at the 200 μM concentration. These 238 compounds were subjected to cocrystallographic analysis in at least one of these three kinases. From this experiment, >100 structures showing bound compound were solved. In particular, Pim-1 provided a robust system for cocrystallizing small low affinity compounds (16), and one of these costructures revealed the binding of 7-azaindole to the ATP-binding site. However, although the heterocycle occupied roughly the position of the adenine ring, multiple binding modes were observed (differing across the four protein monomers in the asymmetric unit), consistent with the weak affinity ($IC_{50} > 200$ μM for Pim-1). Subsequently, a group of mono-substituted 7-azaindoles with increased affinity was synthesized, including the 3-aminophenyl analog ($IC_{50} \approx 100$ μM for Pim-1) that bound to Pim-1 with a single, consistent binding mode (Fig. 1*A*). Overlap of this structure with those of many different kinase family members suggested that this scaffold candidate represented a general framework capable of presenting two hydrogen bonding interactions with the kinase hinge region and several putative sites of substitution (the 2, 3, 4, 5, and 6 positions; Fig. 1) for the optimization of potency and selectivity.

Author contributions: J.T. and J.T.L. contributed equally to this work; J.T., J.T.L., S.-H.K., J.S., K.Y.J.Z., B.L.W., G.H., C.Z., P.N.I., P.H., D.R.A., M.H., and G.B. designed research; J.T., J.T.L., W.W., J.Z., H.C., S.M., R.B., S.G., J.K., N.K.H., K.S., L.L., K.S.M.S., D.F., Y.-L.Z., A.M., H.N., B.L., J.L., I.C., J.R., Y.S., C.L., C.S., R.S., J.C., and B.P. performed research; J.T., J.T.L., W.W., J.Z., H.C., S.M., R.B., S.G., J.K., N.K.H., K.S., L.L., K.S.M.S., D.F., Y.-L.Z., A.M., H.N., B.L., J.L., I.C., J.R., Y.S., C.L., R.S., J.C., S.-H.K., J.S., K.Y.J.Z., B.L.W., G.H., C.Z., P.N.I., P.H., D.R.A., M.H., and G.B. analyzed data; and J.T., J.T.L., S.-H.K., J.S., K.Y.J.Z., B.L.W., G.H., P.N.I., D.R.A., M.H., and G.B. wrote the paper.

Conflict of interest statement: S.-H.K. and J.S. are Plexxikon founders and share holders.

Freely available online through the PNAS open access option.

Data deposition: The atomic coordinates and structure factors have been deposited in the Protein Data Bank, www.rcsb.org (PDB ID codes 3C4C, 3C4D, 3C4E, and 3C4F).

¶To whom correspondence may be addressed. E-mail: joseph.schlessinger@yale.edu, herlynm@wistar.org, or gbollag@plexxikon.com.

This article contains supporting information online at www.pnas.org/cgi/content/full/0711741105/DC1.

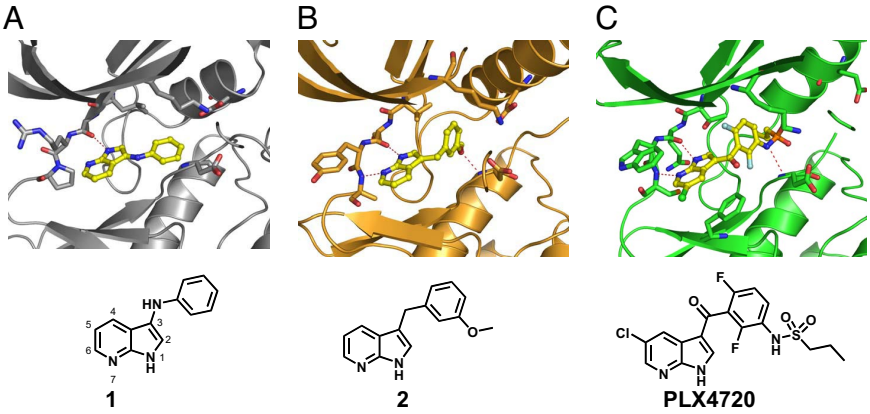

Fig. 1. Structures of individual compounds leading to the discovery of PLX4720 are shown. (*A*) The chemical structure of 3-aminophenyl-7-azaindole (compound 1) is shown beneath its costructure with Pim-1 kinase. (*B*) The chemical structure of 3-(3-methoxybenzyl)-7-azaindole (compound 2) is shown beneath its costructure with the kinase domain of FGFR1. (*C*) The chemical structure of PLX4720 is shown beneath its costructure with B-Raf kinase.

This prediction was confirmed when we determined the costructure of another mono-substituted 7-azaindole bound to the kinase domain of FGFR1 (Fig. 1*B*; IC_{50} = 1.9 μM for FGFR1).

Based on an analysis of structural data for 17 diverse kinases focused on identifying the most productive binding interactions, initial efforts were focused on characterization of compounds substituted at the 3, 4, and 5 positions, resulting in libraries of mono- and di-substituted analogs built around the 7-azaindole core. Subsequent screening of these compounds revealed a set containing a difluoro-phenylsulfonamide substructural motif that displayed excellent potency for oncogenic B-Raf and selectivity against many other kinases, including wild-type B-Raf. These compounds were cocrystallized with engineered forms of $B\text{-}Raf^{V600E}$ and wild-type B-Raf in which solvent-exposed hydrophobic residues have been mutated to increase the level of soluble protein expression in *Escherichia coli*. Based on these cocrystal structures, subsequent optimization chemistry led to the discovery of propane-1-sulfonic acid [3-(5-chloro-1H-pyrrolo[2,3-b]pyridine-3-carbonyl)-2,4-difluoro-phenyl]-amide (PLX4720), whose chemical structure and biochemical characterization are displayed in Fig. 1*C* and Table 1. As evident from this characterization, PLX4720 inhibits $B\text{-}Raf^{V600E}$ kinase activity *in vitro* at 10-fold lower concentrations than wild-type B-Raf. Furthermore, PLX4720 is remarkably selective against a diverse panel of 70 other kinases.

Table 1. Biochemical IC_{50} determinations for PLX4720 versus a panel of kinases

Assay	IC_{50}, nM
B-Raf V600E	13
B-Raf	160
BRK	130
FRK	1,300
CSK	1,500
SRC	1,700
FAK	1,700
FGFR	1,900
KDR	2,300
HGK	2,800
CSF1R	3,300
AURORA A	3,400

Kinases with IC_{50}s > 5,000 nM: ABL1, AKT1, AKT2, AKT3, ALK, BTK, CAMK2A, CDK2/CYCLIN A, CHK1, CHK2, CK1ε, CLK1, EGFR, EPHA2, EPHB4, ERK2, FER, FLT3, GRK2, GSK3β, HCK, IGF1R, IKKβ, IRAK4, JAK3, JNK1, JNK2, JNK3, KIT, MAPKAPK2, MEK1, MER, MET, MKK6, MLK1, MST1, NEK2, P38α, P70S6K, PAK3, PDGFRα, PDK1, PIM1, PKA, PKCμ, PKCθ, PLK1, PYK2, ROCK1, SYK, TAO1, TIE2, TRKA, TSSK1, ZIPK. We are unable to reliably measure wild-type c-Raf-1 activity. However, by using an activated form of c-Raf-1 with Y340D and Y341D mutations, an IC_{50} of 6.7 nM is determined. This suggests that PLX4720 binds with high affinity to the "active" form of both B-Raf and c-Raf-1.

Modes of Inhibitor Interaction and Selectivity. To understand the high affinity and selectivity of PLX4720, we determined the crystal structure of the B-Raf/PLX4720 complex (Fig. 2). Each crystallographic unit contains two asymmetrically packed kinase-inhibitor complexes, suggesting that the inhibitor-bound state may possess an ensemble of conformations. One of the complexes (Fig. 2*C*) superposes well with the published B-Raf/BAY 43-9006 structure (17). As in the published structure, Phe-595 of the DFG motif was displaced by the compound and flipped-out from the ATP-binding pocket (referred to here as the "DFG-out" or inactive conformation). However, because compound occupancy in this conformation is relatively low (60%), this is probably not the most populated conformation of the bound state. Instead, PLX4720 binds preferentially to the second complex (Fig. 2*B*) in the asymmetric unit where compound occupancy is 100%; this appears to be the "active" (or "DFG-in") conformation of the kinase. The critical binding determinant for oncogenic selectivity derives from the interaction between the sulfonamide and the beginning of the DFG region that subsequently directs the attendant alkyl chain into a small pocket unique to the Raf family (termed the "Raf-selective pocket") (Fig. 2*B*). Analysis of the pharmaceutical and pharmacological properties of several analogs led to the selection of the propyl substitution of the sulfonamide found in PLX4720 as that providing the optimal combination of features desirable for an orally administered therapeutic agent.

The specific molecular interactions of PLX4720 to both conformations are shown in Fig. 2 *E* and *F*. PLX4720 binds in the cleft between the N and C lobes of the kinase domain near the hinge region, which overlaps with the ATP-binding site (Fig. 2*A*). Hydrogen bonding of the azaindole to the hinge residues anchors this structure, and the 3-substituent extends toward the activation loop (A-loop). Specifically, N7 serves as hydrogen bond acceptor from the backbone amide of Cys-532, while N1 serves as hydrogen bond donor to the backbone carbonyl of Gln-530. The azaindole is tightly confined within the adenine-binding region of the ATP pocket, surrounded by residues Cys-532, Trp-531, Thr-529, Leu-514, and Ala-481. The small 5-chloro substituent points toward the solvent region with a van der Waal's contact with Ile-463. By contrast, the 3-substituent appears to have extensive interactions with the protein in a binding trajectory that deviates markedly from the bona fide ATP-binding pocket (Fig. 2*A*). Biochemical assays have shown that the ketone linker enhances potency, and the structure reveals that the carbonyl oxygen is accepting an H-bond from a water molecule. The difluoro-phenyl moiety is anchored in a hydrophobic pocket, surrounded by residues Ala-481, Val-482, Lys-483, Val-471, Ile-527, Thr-529, Leu-514, and Phe-583.

While PLX4720 cocrystallizes readily with the wild-type B-Raf protein (Fig. 2) when the V600E-mutant protein is cocrystallized with analogs such as PLX3203 and other mutant-selective analogs, the compound is bound to the DFG-in protein conformation with

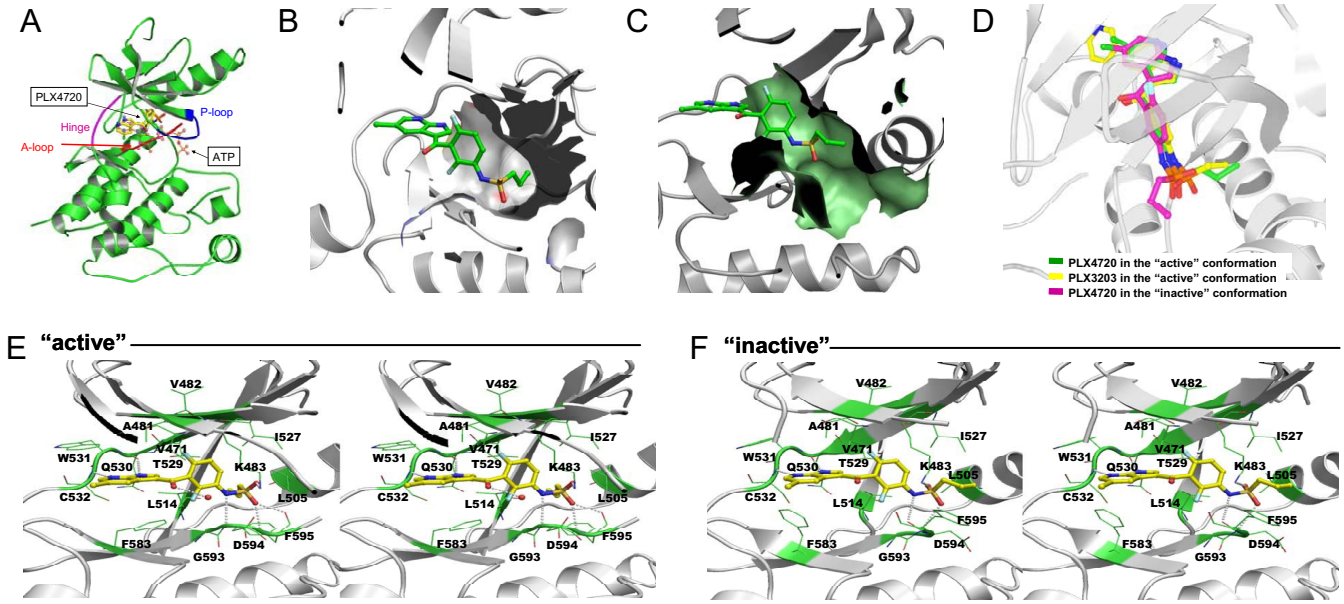

Fig. 2. Depiction of the three-dimensional structure of PLX4720 bound to B-Raf. (*A*) The structure of B-Raf^{V600E} bound to PLX4720 (yellow) is overlayed with an ATP model based on structures of ATP analogs in complex with other tyrosine kinases (orange). This view indicates that the PLX4720 scaffold overlaps with the adenine-binding site, but the tail of PLX4720 binds to a different pocket from the ATP ribose-triphosphate tail. The positions of the hinge, activation loop (A-loop), and phosphate-binding loop (P-loop) are also shown. (*B*) A surface representation shows PLX4720 binding to the B-Raf-selective pocket in the active conformation. (*C*) A surface representation shows PLX4720 binding to the kinase general pocket in the inactive conformation. (*D*) A close-up view shows the overlay PLX4720 bound to both active (green) and inactive (purple) conformations of the V600 protein, and PLX3203 (yellow) bound to V600E protein in the active kinase conformation. (*E*) A stereoview shows the specific interactions of PLX4720 to the active kinase conformation. In this conformation, the phenylalanine of the DFG loop is pointing in toward the compound-binding site. (*F*) A stereoview shows the specific interactions of PLX4720 to the inactive kinase conformation. In this conformation, the phenylalanine of the DFG loop is pointing away from the compound-binding site, and binding of PLX4720 is disfavored, leading to partial occupancy of this site even at the 1 mM compound concentration used in cocrystallography.

almost identical interactions to the structure of the wild-type protein/PLX4720 complex (Fig. 2*D*). By contrast, no PLX3203 electron density is observed in the DFG-out conformation of the V600E protein (data not shown). These structural data support the conclusion that PLX4720 binds preferentially to the active form of B-Raf wild-type and V600E mutant proteins.

Perhaps the key to the activation-state specificity of PLX4720 is the differential interaction of the sulfonamide moiety with the Asp and Phe of the DFG sequence. In the active conformation (Fig. 2*E*), the nitrogen atom of the sulfonamide moiety is within H-bond distance to the main-chain NH group of Asp-594. Such an interaction suggests that the nitrogen atom is deprotonated. Meanwhile, the oxygen atoms of the sulfonamide form H-bonds to the backbone NH of Phe-595 and the side chain of Lys-483. In the DFG-out conformation (Fig. 2*F*), the anchor residue Asp-594 switches conformation, thereby driving the A-loop to block the ATP-binding pocket. Such a conformational switch of the A-loop turns the main chain carbonyl to interact with the nitrogen of the sulfonamide moiety indicating its protonated state. Note that the pK_a of this sulfonamide moiety was experimentally determined to be 7.7, and the crystallization pH is 6.0. These data support a selectivity mechanism by which the deprotonated sulfonamide favors an interaction with the active kinase conformation that is also favored by the V600E mutation.

The propyl group is critical for selective binding to the active conformation of Raf versus other kinases. In the active monomer conformation (Fig. 2*B*), the propyl group of PLX4720 binds to the Raf-selective pocket. Comparison with structures of 80 other kinases showed that very few kinases possess a similar pocket at this exact location. The presence of this pocket in B-Raf^{V600E} appears to require an outward movement of the αC helix. As a result, although B-Raf^{V600E} in the active conformation shares the same DFG conformation as the structure of activated B-Raf (10), the orientation of the αC helix is significantly different between the two structures. Because Glu-501 of the αC helix is separated from the catalytic Lys-483, PLX4720 appears to have trapped the oncogenic B-Raf kinase in a unique conformation. Decreasing the steric size of the propyl group selectively decreases the ability to inhibit the inactive protein, resulting in increased selectivity for the active form. Conversely, compounds such as BAY 43–9006 (17) with large tail groups bind to an alternative pocket that is present only when the protein is in the inactive conformation. This alternative pocket (Fig. 2*C*) is highly conserved in many kinases and is therefore termed the "kinase general pocket." Although PLX4720 can bind to both conformations, the preference for the active conformation and corresponding access to the Raf-selective pocket plays a key role in the selectivity against non-Raf kinases.

Cellular Selectivity in Multiple Tumor Lines. The identification of a B-Raf^{V600E}-selective compound enables exploration of the physiological role of the *BRAF^{V600E}* oncogene. It is clear from Table 2 that tumor cell lines bearing the *BRAF^{V600E}* oncogene are significantly more sensitive to inhibition by PLX4720. Despite the observation that PLX4720 is 10-fold selective for the B-Raf^{V600E} kinase in enzymatic assays, the cellular selectivity can exceed 100-fold. This finding is consistent with the report of similar selectivity for the *BRAF^{V600E}*-bearing cells in experiments using specific inhibitors of MEK (18) and B-Raf (10). Indeed, the results point to a critical role of the Raf-MEK-ERK pathway in *BRAF^{V600E}*-bearing cells that can be bypassed in cells lacking oncogenic *BRAF*.

To further explore the differential biology of tumor cells with or without oncogenic *BRAF*, direct analysis of the Raf-MEK-ERK pathway was explored. By using the selective MEK inhibitor PD0325901, ERK phosphorylation as a read out of the Raf-MEK-ERK pathway was potently inhibited in all cell lines (Table 2), consistent with previous studies (18). By contrast, ERK phosphor-

Table 2. Cellular GI_{50} determinations for PLX4720 versus a panel of cell lines

Cell line	B-Raf sequence	PLX4720 proliferation GI_{50}, μM	PLX4720 P-ERK GI_{50}, μM	PD0325901 P-ERK GI_{50}, μM
COLO205	V600E	0.31	0.014	<0.002
A375	V600E	0.50	0.046	<0.002
WM2664	V600D	1.5		
COLO829	V600E	1.7	0.044	<0.002
HT716	Wild type	10		
SW620	Wild type	13	>40	<0.002
H460	Wild type	24		
Calu-6	Wild type	26		
HCT116	Wild type	27		
SK-MEL2	Wild type	27	23	<0.002
SK-MEL3	Wild type	27		
Lovo	Wild type	29		
H1299	Wild type	41		

ylation is differentially affected by a 1-h treatment with PLX4720: in cells bearing the *BRAF*^{V600E} oncogene ERK, phosphorylation is potently inhibited, whereas ERK phosphorylation is unaffected in cells that lack the *BRAF* oncogene. This observation is consistent with previous reports of a negative feedback pathway from ERK through c-Raf-1 (13, 19). Increased ERK activity results in increased phosphorylation of c-Raf-1, thereby autolimiting the flux through the Raf-MEK-ERK pathway. We speculate that this negative feedback loop is lost in *BRAF*^{V600E}-bearing tumor cells, resulting in the pronounced dependence of these cells on the Raf-MEK-ERK pathway. Note that certain premalignant cells such as those found in benign nevi also demonstrate frequent expression of B-Raf^{V600E} (20, 21), and it remains unclear how these cells avoid transformation to a malignant state. Recent evidence supports the link between the negative feedback and oncogene-induced senescence (22). Perhaps it is the negative feedback that prevents the

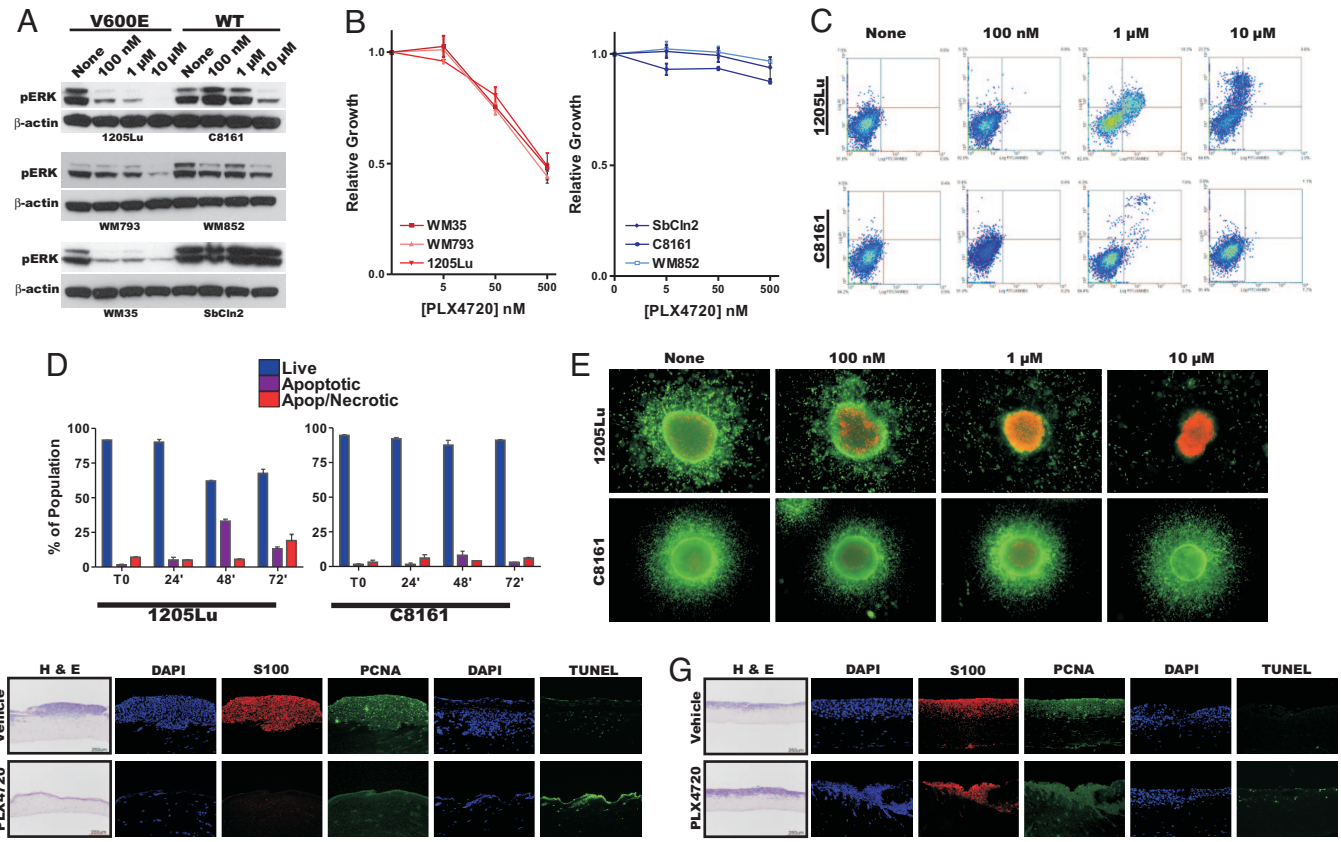

Fig. 3. Selectivity and antimelanoma activity of PLX4720 *in vitro*. (*A*) Panel of melanoma cell lines (V600E+, left; B-Raf wild-type, right) were treated with various dosages of PLX4720, and protein extracts were subject to immunoblotting. Activity within the MAPK pathway is represented by levels of phosphorylated ERK; β-actin serves as a loading control. (*B*) B-Raf V600E+ (*Left*) and B-Raf wild-type (*Right*) cells were treated PLX4720 at the indicated dosages for 72 h. Cell number was assayed by MTT analysis. (*C*) 1205Lu and C8161 cells were treated with 1 μM PLX4720 for the times indicated and stained with Annexin V/FITC and propidium iodide (PI) for analysis of apoptosis. (*D*) Graphs represent raw data from the Annexin/PI assay. (*E*) Spheroids from 1205Lu and C8161 cells were treated with indicated dosages of PLX4720 and stained with calcein AM and ethidium bromide to assess overall viability. Green (calcein-AM) indicates live cells; red (EtBr) depicts apoptotic cells. (*F*) Synthetic skin was created by using 1205Lu (V600E+) cells and subjected to vehicle control (*Upper*) or 1 μM PLX4720 (*Lower*) for 72 h. H&E staining is depicted (*Left*), and immunofluorescent stains for DAPI, PCNA, and S100 are also shown. (*G*) Same as *F*, except with C8161 (B-Raf wild-type) cells.

transformation process, and loss of the feedback is critical to malignancy.

Melanoma Cell Biology. To further explore the role of B-Raf^{V600E} in melanoma, the effects of PLX4720 on a larger panel of melanoma cell lines were investigated. PLX4720 inhibited ERK activity only in those cell types that harbor the V600E mutation whereas ERK remained unaffected in cells with wild-type B-Raf (Fig. 3*A*). Furthermore, only those cell lines containing the V600E gene product displayed decreased growth rates, whereas melanoma cells and primary melanocytes [supporting information (SI) Fig. 5] expressing wild-type B-Raf grew at similar rates to the nontreated controls (Fig. 3*B*). Of the cell lines tested, the 1205Lu (B-Raf^{V600E}) and C8161 (B-Raf wild-type) cells represent highly malignant examples that are inherently resistant to pharmacological intervention (23); consequently, these cell lines were chosen for further study.

Cell-cycle analyses established that PLX4720 is sufficient to induce cell-cycle arrest at 24 h posttreatment in the B-Raf^{V600E} 1205Lu cells, but not the B-Raf wild-type C8161 melanoma cells (SI Fig. 6). B-Raf^{V600E} cells were also highly susceptible to apoptotic induction, whereas wild-type B-Raf melanoma cells remained unaffected even by prolonged exposure to the drug (Fig. 3 *C* and *D*). The collective data, therefore, suggest that PLX4720 has antimelanoma activity only against cells that harbor the V600E mutation.

Others have reported that chemotoxic compounds possess differential capacities to inhibit growth and/or induce apoptosis that depends on the cell's interaction with the immediate microenvironment (24, 25). We confirmed the results from our two-dimensional platforms by using live/dead spheroid analyses to determine the effect(s) of PLX4720 on melanoma cells in the context of extracellular matrices, such as collagen I. Indeed, treatment with PLX4720 over 72 h confirmed that mutant B-Raf cells undergo apoptosis in response to the compound to a much greater degree than their wild-type counterparts (Fig. 3*E*).

It is possible to grow synthetic skin that accurately recapitulates the epidermal architecture of the skin, including extracellular matrices, relevant cell types, and their proximal localization to one another (26, 27). Melanoma-based synthetic skin is characterized by an overabundance of melanoma cells that eventually overtakes the outermost layer of keratinocytes. Here, artificial skin was synthesized by using the 1205Lu or C8161 melanoma cell lines, rather than melanocytes. Subsequently, PLX4720 was administered to ascertain the effects of the compound on the various cellular components of melanoma lesions. In the absence of PLX4720, both melanomas grew well (Fig. 3 *F* and *G*). The B-Raf^{V600E} 1205Lu cells were significantly inhibited in the presence of the drug, as evidenced by the thin melanoma layer and existence of the outer keratinocyte layer (Fig. 3*F*); growth of the C8161 B-Raf wild-type cells, however, was unaffected by PLX4720 treatment (Fig. 3*G*). Immunofluorescent analyses confirmed that the C8161-based reconstructs showed similar patterns of staining for the proliferation marker, PCNA, in both untreated and treated samples (Fig. 3*G*). Conversely, the B-Raf^{V600E} -based synthetic skin displayed a drastic decrease in PCNA staining when in the presence of PLX4720 (Fig. 3*F*). Skin reconstructs were also stained with TUNEL to indicate areas of high apoptosis; TUNEL staining was inversely correlated to PCNA staining exclusively in PLX4720-treated B-Raf^{V600E} reconstructs, as expected (Fig. 3*F*). The collective data from these reconstruct studies strongly suggest that PLX4720 initiates an apoptotic response only in cells with the V600E mutation.

Animal Efficacy. To achieve optimal anticancer effects, it is most desirable to cause frank tumor regressions. A tumor xenograft model was explored by using COLO205 cells (that bear the *BRAF^{V600E}* mutation) in nude mice. As shown in Fig. 4*A*, treatment of tumor-bearing mice with 20 mg/kg PLX4720 by using once-daily

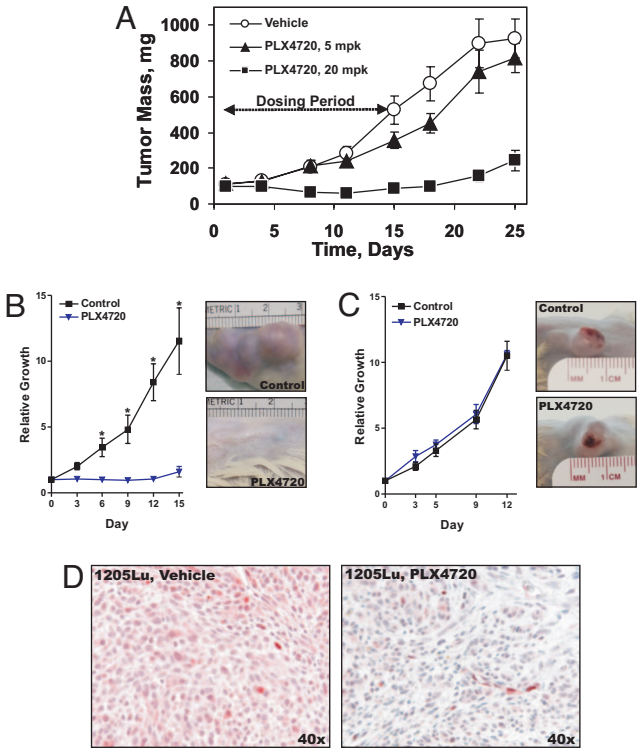

Fig. 4. Effect of PLX4720 on xenograft tumor growth. (*A*) Tumor volume measurements of COLO205 xenograft tumors treated with 5 or 20 mg/kg PLX4720 by oral gavage or treated with vehicle. Dosing occurred from days 1 to 14. (*B* and *C*) Two million cells [1205Lu (*B*); C8161 (*C*)] were s.c. injected into SCID mice. After reaching sufficient size, mice were treated by oral gavage with vehicle control (*Left*) or 100 mg/kg PLX4720 (*Right*) twice daily for the indicated times. (D) 1205Lu xenograft tumors were extracted, fixed in formalin, and paraffin embedded. Vehicle- (*Left*) and PLX4720- (*Right*) treated samples were immunostained for phospho-ERK.

oral dosing resulted in substantial block of tumor growth. Indeed, during the treatment period of 14 days, four of the nine treated mice achieved tumor regressions to below palpable levels. These tumors returned upon cessation of treatment, so some tumor cells were still remaining in these mice. Nonetheless, the 14-day treatment resulted in a 21-day tumor growth delay. A lower 5 mg/kg dose of PLX4720 had a very modest effect on tumor growth. To demonstrate *in vivo* target modulation, phospho-ERK levels were measured in treated tumors 2 h after the final dose of 20 mg/kg PLX4720 on day 14. By using immunohistochemistry for total ERK levels to normalize the data, it was estimated that ERK phosphorylation was inhibited by 43% (data not shown). Although we see no evidence of apoptosis in cellular assays in COLO205 cells treated with PLX4720, the compound clearly can cause regression of tumors *in vivo*. The treatment with PLX4720 was well tolerated, and no adverse effects on any clinical parameters, including body weight, were noted. Indeed, increasing doses of PLX4720 up to 1,000 mg/kg resulted in increasing plasma levels (up to 600 μM) without any evidence of adverse reactions.

Xenograft studies were also performed by using either 1205Lu or C8161 cells in SCID mice. The striking results indicate that oral administration of PLX4720 is sufficient to prevent tumor growth in B-Raf^{V600E} tumors; furthermore, those tumors were nearly, and in some cases completely, destroyed by treatment with PLX4720 (Fig. 4*B*). The growth of B-Raf wild-type tumors remained unaffected by treatment with PLX4720 (Fig. 4*C*). Immunohistochemical assays demonstrated that signals transduced by the MAPK pathway are decreased in those cells harboring the V600E mutation (Fig. 4*D*), thus supporting the notion that the target of the compound was

affected by treatment with PLX4720. The results from these *in vivo* models validate our *in vitro* data and thereby support the use of PLX4720 as a next-generation therapeutic for patients with advanced-stage melanoma.

Conclusions

The mechanism of activating protein kinases by stabilizing the catalytically preferred conformation is exploited by oncogenic mutations such as B-Raf^{V600E}. Conversely, the selective targeting of the active DFG conformation can also be achieved by small-molecule inhibitors, and this should enable the development of future therapeutic kinase inhibitors. The discovery of PLX4720 opens the door to future studies that seek to measure the effects of selective inhibition of B-Raf^{V600E}. Pharmacologic inhibition of oncogenic B-Raf blocks proliferation and causes tumor regressions. This finding is also consistent with recent studies showing the genetic depletion of B-Raf in B-Raf^{V600E}-bearing xenografted melanoma cells results in dramatic tumor regressions (28). Importantly, this efficacy is achieved without apparent toxicity to untransformed cells *in vitro* or to treated mice. The pharmaceutical properties of PLX4720 enable advancement to human clinical trials, with the hope of achieving clinical benefit and maintaining a significant therapeutic window. PLX4720 thus represents perhaps a first-in-class therapeutic molecule that selectively inhibits a target that exists only in tumors.

Experimental Procedures

Note that detailed methods are included as *SI Methods*.

Synthesis of B-Raf Inhibitors. PLX4720 was synthesized by reacting commercially available 5-chloro-7-azaindole with propane-1-sulfonic acid (2,4-difluoro-3-formyl-phenyl)-amide followed by oxidation (SI Scheme 1). Similar procedures were used to synthesize the inhibitors listed in Fig. 1*C* by using appropriately substituted 7-azaindole and aldehyde as starting materials (SI Scheme 2). Detailed synthetic methods are included as *SI Methods*.

Cloning, Expression, Purification, and Crystallization of B-Raf. To enable crystallization, the *BRAF* cDNAs (both V600 and E600) fragment encoding amino acid residues 448–723 with 16 mutations to improve expression (I543A, I544S, I551K, Q562R, L588N, K630S, F667E, Y673S, A688R, L706S, Q709R, S713E, L716E, S720E, P722S, K723G) were cloned into a pET vector (Invitrogen), in frame with a N-terminal histidine tag for bacterial expression. The protein was expressed in *E. coli* cells with an overall yield of 5–10 mg/liter.

B-Raf kinase was expressed, purified, crystallized, and the structures determined by using methods similar to those used for the reported for Pim-1 and Met (16). For enzymatic activity, B-Raf (residues D448–K723) with or without the V600E mutation and fused at the N terminus with six-residue HIS-tag, was coexpressed with CDC37 in insect cells by using a baculovirus vector. For comparative enzymatic determinations, c-Raf-1 (residues Q307–F648, with Y340D and Y341D mutations, fused at N terminus with GST) from baculovirus-infected insect cells was used. For crystallographic data and refinement statistics, see SI Table 3.

Biochemical and Cellular Assays. The *in vitro* Raf kinase activities were determined by measuring phosphorylation of biotinylated-MEK protein by using AlphaScreen Technology (16). In addition, 58 selected kinases were profiled for inhibition by PLX4720 by using the Z′-LYTE biochemical assay format (SelectScreen; Invitrogen) according to the manufacturer's instructions.

Cellular phosphorylation of ERK was determined by immunoassay, and cellular proliferation was determined by using the CellTiter-Glo Luminescent Cell Viability Assay (Promega). Melanoma cell proliferation, cell cycle analysis, apoptosis assay, three-dimensional spheroid growth, and skin reconstruction experiments were carried out as previously described (26, 27).

COLO205 Tumor Xenograft. Female athymic mice (NCr nu/nu; Taconic) were implanted s.c. on day 0 with 30–60 mg COLO205 tumor fragments. Treatments began on day 11, when the mean estimated tumor mass was 104 mg (range, 95–113 mg). All animals were dosed with vehicle (5% DMSO, 1% methylcellulose) or PLX4720 suspended in vehicle by gavage daily for 14 consecutive days. Tumor burden (mg) was estimated from caliper measurements. This study was conducted by Molecular Imaging Research (MIR), and all procedures were approved by the MIR Animal Care and Use Committee.

Melanoma Tumor Xenografts. Metastatic melanoma cells (2×10^6) were s.c. injected into the flanks of SCID mice and allowed ≈2 weeks to reach 0.125 mm^3 in volume. Subsequently, the animals received either 100 mg/kg PLX4720 (oral gavage) or vehicle control twice daily for 15 days. Tumor volume was recorded every 72 h. The average tumor size for each respective group was normalized to the tumor volume at the first day of treatment. After 15 days of treatment, animals were killed and tumors were excised, fixed in formalin, paraffin-embedded, and analyzed by immunohistochemistry.

ACKNOWLEDGMENTS. Diffraction data were collected at the Advanced Light Source and the Stanford Synchrotron Radiation Laboratory, which are supported by the U.S. Department of Energy, Office of Basic Energy Sciences under contract DE-AC03-76SF00098 and DE-AC03-76SF00515, respectively. This work was supported by National Institutes of Health Grants CA 880999 and CA 47159 (to M.H.), AR 051448 (to J.S.), AR 051886 (to J.S.), and P50 AR0504086 (to J.S.). J.L.T. was supported by an Institutional Research Training Grant (T32) CA 09171.

1. Davies H, *et al.* (2002) Mutations of the BRAF gene in human cancer. *Nature* 417:949–954.
2. Samowitz WS, *et al.* (2005) Poor survival associated with the BRAF V600E mutation in microsatellite-stable colon cancers. *Cancer Res* 65:6063–6069.
3. Riesco-Eizaguirre G, *et al.* (2006) The oncogene BRAFV600E is associated with a high risk of recurrence and less differentiated papillary thyroid carcinoma due to the impairment of Na+/I- targeting to the membrane. *Endocr Relat Cancer* 13:257–269.
4. Houben R, *et al.* (2004) Constitutive activation of the Ras-Raf signaling pathway in metastatic melanoma is associated with poor prognosis. *J Carcinog* 3:6–18.
5. Sawyers C (2004) Targeted cancer therapy. *Nature* 432:294–297.
6. Baselga J (2006) Targeting tyrosine kinases in cancer: the second wave. *Science* 312:1175–1178.
7. Card GL, *et al.* (2005) A family of phosphodiesterase inhibitors discovered by cocrystallography and scaffold-based drug design. *Nat Biotechnol* 23:201–207.
8. Smith RA, Dumas J, Adnane L, Wilhelm SM (2006) Recent advances in the research and development of RAF kinase inhibitors. *Curr Top Med Chem* 6:1071–1089.
9. Niculescu-Duvaz I, *et al.* (2006) Novel inhibitors of B-RAF based on a disubstituted pyrazine scaffold. Generation of a nanomolar lead. *J Med Chem* 49:407–416.
10. King AJ, *et al.* (2006) Demonstration of a genetic therapeutic index for tumors expressing oncogenic BRAF by the kinase inhibitor SB-590885. *Cancer Res* 66:11100–11105.
11. Lyons JF, Wilhelm S, Hibner B, Bollag G (2001) Discovery of a novel Raf kinase inhibitor. *Endocr Relat Cancer* 8:219–225.
12. Lackey K, *et al.* (2000) The discovery of potent cRaf1 kinase inhibitors. *Bioorg Med Chem Lett* 10:223–226.
13. Hall-Jackson CA, *et al.* (1999) Paradoxical activation of Raf by a novel Raf inhibitor. *Chem Biol* 6:559–568.
14. Li N, Batt D, Warmuth M (2007) B-Raf kinase inhibitors for cancer treatment. *Curr Opin Investig Drugs* 8:452–456.
15. Wilhelm SM, *et al.* (2004) BAY 43–9006 exhibits broad spectrum oral antitumor activity and targets the RAF/MEK/ERK pathway and receptor tyrosine kinases involved in tumor progression and angiogenesis. *Cancer Res* 64:7099–7109.
16. Kumar A, *et al.* (2005) Crystal structures of proto-oncogene kinase Pim1: A target of aberrant somatic hypermutations in diffuse large cell lymphoma. *J Mol Biol* 348:183–193.
17. Wan PT, *et al.* (2004) Mechanism of activation of the RAF-ERK signaling pathway by oncogenic mutations of B-RAF. *Cell* 116:855–867.
18. Solit DB, *et al.* (2006) BRAF mutation predicts sensitivity to MEK inhibition. *Nature* 439:358–362.
19. Dougherty MK, *et al.* (2005) Regulation of Raf-1 by direct feedback phosphorylation. *Mol Cell* 17:215–224.
20. Pollock PM, *et al.* (2003) High frequency of BRAF mutations in nevi. *Nat Genet* 33:19–20.
21. Michaloglou C, *et al.* (2005) BRAFE600-associated senescence-like cell cycle arrest of human naevi. *Nature* 436:720–724.
22. Courtois-Cox S, *et al.* (2006) A negative feedback signaling network underlies oncogene-induced senescence. *Cancer Cell* 10:459–472.
23. Smalley KS, *et al.* (2006) Multiple signaling pathways must be targeted to overcome drug resistance in cell lines derived from melanoma metastases. *Mol Cancer Ther* 5:1136–1144.
24. Desoize B, Gimonet D, Jardiller JC (1998) Cell culture as spheroids: an approach to multicellular resistance. *Anticancer Res* 18:4147–4158.
25. Durand RE (1989) Distribution and activity of antineoplastic drugs in a tumor model. *J Natl Cancer Inst* 81:146–152.
26. Hsu MY, *et al.* (2000) E-cadherin expression in melanoma cells restores keratinocyte-mediated growth control and down-regulates expression of invasion-related adhesion receptors. *Am J Pathol* 156:1515–1525.
27. Meier F, *et al.* (2000) Human melanoma progression in skin reconstructs: Biological significance of bFGF. *Am J Pathol* 156:193–200.
28. Hoeflich KP, *et al.* (2006) Oncogenic BRAF is required for tumor growth and maintenance in melanoma models. *Cancer Res* 66:999–1006.